BBA - Biomembranes 1864 (2022) 183997

Contents lists available at ScienceDirect

BBA - Biomembranes

journal homepage: www.elsevier.com/locate/bbamem

Homogeneous hybrid droplet interface bilayers assembled from binary mixtures of DPhPC phospholipids and PB-*b*-PEO diblock copolymers

Subhadeep Koner [a], Joseph Tawfik [a], Farzin Mashali [a], Kristen B. Kennison [b], William T. McClintic [b], Frederick A. Heberle [b], Yu-Ming Tu [c], Manish Kumar [d,e], Stephen A. Sarles [a,*]

[a] Department of Mechanical Aerospace and Biomedical Engineering, University of Tennessee, Knoxville, TN 37996, USA
[b] Department of Chemistry, University of Tennessee, Knoxville, TN 37996, USA
[c] Department of Chemical Engineering, Massachusetts Institute of Technology, Cambridge, MA, USA
[d] McKetta Department of Chemical Engineering, The University of Texas at Austin, Austin, TX 78712, USA
[e] Department of Civil, Architectural and Environmental Engineering, The University of Texas at Austin, Austin, TX 78712, USA

ARTICLE INFO

Keywords:
Hybrid membrane
Diblock copolymer
Polybutadiene-b-polyethylene oxide (PBPEO)
Diphythanoyl phosphatidylcholine (DPhPC)
Droplet interface bilayer
Alamethicin

ABSTRACT

Hybrid membranes built from phospholipids and amphiphilic block copolymers seek to capitalize on the benefits of both constituents for constructing biomimetic interfaces with improved performance. However, hybrid membranes have not been formed or studied using the droplet interface bilayer (DIB) method, an approach that offers advantages for revealing nanoscale changes in membrane structure and mechanics and offers a path toward assembling higher-order tissues. We report on *hybrid* droplet interface bilayers (hDIBs) formed in hexadecane from binary mixtures of synthetic diphytanoyl phosphatidylcholine (DPhPC) lipids and low molecular weight 1,2 polybutadiene-b-polyethylene oxide (PBPEO) amphiphilic block copolymers and use electrophysiology measurements and imaging to assess the effects of PBPEO in the membrane. This work reveals that hDIBs containing up to 15 mol% PBPEO plus DPhPC are homogeneously mixtures of lipids and polymers, remain highly resistive to ion transport, and are stable—including under applied voltage. Moreover, they exhibit hydrophobic thicknesses similar to DPhPC-only bilayers, but also have significantly lower values of membrane tension. These characteristics coincide with reduced energy of adhesion between droplets and the formation of alamethicin ion channels at significantly lower threshold voltages, demonstrating that even moderate amounts of amphiphilic block copolymers in a lipid bilayer provide a route for tuning the physical properties of a biomimetic membrane.

1. Introduction

The many active and passive functions performed by cellular membranes motivate the need for effective materials and methods to obtain biomimetic model membranes with similar capabilities. For example, biomimetic membranes in the form of spherical vesicles and planar bilayers are needed for researching biophysical mechanisms related to selective transport, ion channel gating, and stimuli-responsive transmembrane signaling. They are also key to developing functional materials that offer either similar capabilities to membranes or controlled interactions with cellular interfaces. Such technologies hold significant promise for applications such as biosensing [1], nanoparticle-assisted drug delivery [2,3], DNA sequencing [4], artificial tissue development [5], and desalination and bio-separations [6–8].

Biomimetic membranes are usually assembled from either phospholipids (PL) [9,10] or amphiphilic block copolymers (BCP) [11–14] (e.g., diblock or triblock architectures with alternating hydrophilic and hydrophobic blocks) organized into a bilayer. Amphiphilic BCPs are most frequently constructed from poly(2-methyl oxazoline) (PMOXA) or poly(ethylene oxide) (PEO) hydrophilic groups, linked to poly(butadiene) (PB), poly(dimethyl siloxane) (PDMS), or poly(isoprene) (PI) hydrophobic blocks [15,16]. While synthetic or naturally-derived PL closely resemble lipid compositions in cells and yield membranes with similar dimensions and physical properties, their use ex vivo is often curtailed by chemical degradation, higher permeability, and limited mechanical strength (e.g., bending rigidity, lysis strain) [17–20]. In contrast, while many BCP-based membranes hold advantages in these same metrics, using BCP in place of PL can result in artificially large

* Corresponding author.
E-mail address: ssarles@utk.edu (S.A. Sarles).

https://doi.org/10.1016/j.bbamem.2022.183997
Received 28 December 2021; Received in revised form 9 June 2022; Accepted 14 June 2022
Available online 16 June 2022

hydrophobic thicknesses [21,22] and reduced lateral fluidity [17], which limit the ability to host transmembrane biomolecules for selective signaling and transport.

Alternatively, hybrid membranes combine BCP and PL, seeking to leverage the most favorable properties of each constituent in the resulting biomimetic membrane. This approach has been taken by several groups, many of which used PB-*b*-PEO BCPs in combination with phosphatidylcholine (PC) lipids [17,21,23–35]. The results from these studies demonstrate that hybrid PL-BCP membranes in the form of vesicles or planar bilayers can exhibit properties superior to PL-only or BCP-only models [28]. Depending on the types of PL and BCP used and their relative fractions in the membrane, hybrid membranes can exist as homogeneous mixtures or as laterally phase-separated PL and BCP domains. Thus, the local environment (e.g. hydrophobic thickness, lateral fluidity, chemical functionality) of a hybrid membrane can be tailored to recognize membrane-active species [25] and host ion channels formed from peptides [36] or integral membrane proteins, including cytochrome bo_3 [37], OmpF [32,38], potassium-selective [35], and mechanosensitive [39] ion channels, while also improving the global characteristics (e.g., permeability, stability, dehydration resistance) [17,27,28,40]. However, the benefits of hybrid membranes may not materialize until methods to assemble and comprehensively assess them move beyond closed vesicles and fragile planar bilayers.

The droplet interface bilayer (DIB) technique permits assembling a fluid bilayer membrane between two surfactant-coated water droplets immersed in oil [41–43]. Compared to planar membranes painted across apertures or resting on solid surfaces, a DIB membrane (or *DIB*) offers key advantages: a simpler formation that demands less user skill, greater longevity due to removed interactions with a substrate, independent aqueous volumes needed to perform electrophysiology and establish leaflet asymmetry, and direct control over bilayer area. These plusses translate into greater control for use in a wide variety of experimental studies. Hence DIBs have been used by microbiologists, chemists, and physicists to explore in situ a variety of basic biophysical questions and processes [44–47] as well as by engineers to develop biomimetic sensors [48,49], energy conversion devices [50,51], and even brain-inspired computing elements [52–55]. Moreover, because an adhesive droplet-based approach is inherently modular, the DIB technique translates well to microfluidic environments for high throughput analyses [56–58] and it permits connecting many droplets to construct 3D tissue-like synthetic materials [59–61]. In the latter, droplet networks enabled by bilayer-stabilized adhesive droplets result in a compartmentalized soft material that closely mimics the hierarchy of living cells and tissues achieved via membrane barriers. This approach at synthetic tissues establishes the potential to obtain emergent functional properties within biological membrane-inspired—and perhaps biocompatible materials—that sense, actuate, learn, and remember.

DIBs are typically formed from either synthetic PL or natural lipid extracts. Far less research has been reported on assembling DIBs from non-PL surfactants, such as BCPs, despite the potential payoff of improved biomimetic membranes. We previously examined the dynamics of DIB formation using ABA-type triblock copolymers, which exhibited voltage-triggered reversible adhesion [62,63]. This behavior resulted from the hair-pin arrangements of the surfactants at the oil-water interface. Depending on the oil, these bilayer interfaces exhibited hydrophobic thicknesses of 10–20 nm, far too thick for supporting transmembrane species (e.g., proteins, ion channels) needed to selectively regulate transport between compartments. This work reiterated the importance of molecular-scale interactions between the solvent and the hydrophobic portion of the BCP molecule in determining whether bilayer formation (via oil exclusion from between droplets) is energetically favorable [62]. Alternatively, our attempts to assemble DIBs from similar types of diblock BCP (e.g., PMOXA-*b*-PDMS, PDMS-*b*-PEO, MW $\geq$ 2 kDa) have thus far failed to yield stable polymeric DIBs.

Motivated by the potential advantages of hybrid membranes and the opportunity to investigate them using electrophysiology and the DIB technique, we report on *hybrid DIBs* (hDIBs) assembled in hexadecane from symmetric binary mixtures of DPhPC phospholipids and PBPEO diblock copolymers, components that individually yield membranes with low permeabilities to small molecules, ions, and water [40,45]. The diblock selected for this study is a carboxylic acid terminated 1,2 poly (butadiene)-*co*-poly(ethylene oxide) copolymer (PBPEO from here on). We chose a low molecular weight (short-chain) variant ($PB_{12}PEO_8$-COOH, MW $\sim$ 1000 g/mol) because it results in sufficiently thin polymer bilayer membranes capable of hosting both biological OmpF membrane proteins [64,65] and artificial transmembrane channels [66]. The objectives of the study are to use a combination of simultaneous electrical measurements and imaging to characterize the effects of PBPEO concentration on the equilibrium physical properties (e.g., electrical resistance, thickness, stability under voltage, membrane tension, and adhesion energy), the distribution of PBPEO within the bilayer, and the insertion of voltage-activated ion channels in DPhPC:PBPEO hDIBs. This approach shows how electrical measurements of hDIBs can reveal greater understanding of the effects of BCPS in hybrid membranes.

2. Materials & methods

2.1. Materials

The aqueous droplets used to construct DIBs consisted of mixed PL: BCP vesicles, salt, and buffering agent in 99.99 % pure deionized water. Potassium chloride (KCl), 3-(*N*-morpholino) propanesulfonic acid (MOPS), sodium hydroxide (NaOH), agarose ($C_{12}H_{18}O_9$), sucrose, *n*-hexadecane (99 % pure), ethanol, and isopropyl alcohol were purchased from Sigma Aldrich. DPhPC lipids (>99 % purity) were obtained from Avanti Polar Lipids, Inc. and used without further purification. The diblock material used in this work is a carboxylic acid terminated 1,2 polybutadiene-*block*-polyethylene oxide (PB_{12}-*b*-PEO_8-COOH, MW $\sim$ 1000 g/mol, PDI = 1.18) synthesized via anionic polymerization as described elsewhere [64].

2.2. Large unilamellar vesicles (LUVs) preparation

To prepare a solution of hybrid LUVs, PBPEO was first solvated in chloroform at a concentration of 10 mg/mL and then mixed with DPhPC lipids dissolved in chloroform at the desired lipid:polymer molar ratio. The chloroform was then evaporated, first using a gentle nitrogen stream and then under vacuum for 3 h. Once the solvent fully evaporated, the lipid:polymer film was then rehydrated in 500 mM KCl, 10 mM MOPS, pH 7 to a final lipid concentration of 2 mg/mL (see Table S1 in the supplementary information (SI) for total amphiphile concentrations of mixed vesicle solutions). The hydrated suspension was subjected to 5 freeze-then-thaw cycles with passive cooling and heating at −20 °C and ~20 °C, respectively, to create a solution of multilamellar vesicles. LUVs were formed by extrusion, using 11 passes through a 100 nm-pore polycarbonate membrane (Whatman) in an Avanti Mini Extruder. Zeta potential measurements (Table S1) show that the addition of PBPEO, which contains a negatively charged COOH group, does not significantly affect the surface charge of an LUV. Extruded LUV solutions were stored at 4 °C until further use.

2.3. DIB formation

DIBs were formed at room temperature (22 °C) between two, 300 nL aqueous droplets of LUV solution suspended on agarose-coated wire-type electrodes in an oil-filled reservoir as described elsewhere [67]. The oil reservoir and droplets were centered above a 4× objective lens on an inverted microscope. The positions of both electrodes were controlled by manual, three-axis micromanipulators. A lipid bilayer was formed by bringing droplets into contact following a brief incubation period to ensure monolayer assembly. To aid in holding droplets, electrodes were

lowered in the oil such that the bottom of the droplets gently rest on the substrate. Bottom-view images (Fig. 1A) of connected droplets were obtained using a QIClick-F-M-12-C (SN: Q31274) camera controlled by Micromanager software. Side view images of connected droplets (Fig. S1 in the SI) were obtained using an IDS-UI-3360CP-M_GL R2 camera controlled by IDS Software Suite. Images from both views were used to estimate bilayer area for computing specific capacitance and thickness as described elsewhere [68].

2.4. Giant unilamellar vesicles (GUVs) formation and confocal imaging

Giant unilamellar vesicles (GUVs) were formed via gel-assisted swelling. PBPEO and DPhPC dissolved in chloroform are mixed at various PL:BCP molar ratios: 100:0, 90:10, 80:20, and 50:50. Nile Red hydrophobic dye was added to all mixtures at a final concentration of 0.1 mol%. A petri dish was plasma cleaned for 1 min and then spin-coated with a warm 1 wt/vol% agarose solution, which was left to dry at room temperature. Small droplets of lipid/BCP mixture were deposited onto the agarose coated petri dish that was then placed under a gentle stream of nitrogen for a few min and then in a desiccator for 1 h to evaporate the chloroform. The GUV growth buffer containing 400 mM sucrose in water was added and left for 30 min for swelling to proceed and form GUVs. For harvesting the GUVs, the narrow end of a 100 μL pipette tip was cut to create a larger opening and avoid damaging GUVs. Confocal fluorescence imaging was performed at room temperature using a Nikon C2+ point scanning system with a 561 nm laser line attached to a Nikon Eclipse Ti2-E microscope equipped with a Plan Apo Lambda 60× oil immersion objective.

2.5. Electrophysiology

Bilayer current measurements were made using an Axopatch 200B patch-clamp amplifier and Digidata 1440A data acquisition system (Molecular Devices). All recordings were made at room temperature with appropriate shielding using a well-grounded Faraday cage in place to minimize noise. Voltage waveforms were generated using either a Hewlett-Packard 3314A function generator or a National Instruments Compact DAQ with a NI 9263 analog output module controlled by a custom LabVIEW script. Voltages from these sources were sent to the headstage of the Axopatch 200B via the external input to the amplifier. Current measurements were lowpass filtered at 1 kHz on the Axopatch 200B and then sampled at 20 kHz. All data were processed using Matlab.

2.6. Monolayer formation and interfacial tension measurement

Pendant drop tensiometry was performed on a Dataphysics OCA 15EC to assess monolayer formation at the oil-water interface, including measuring equilibrium tension. A Teflon-coated blunt tip needle with a 0.72 mm inner diameter was used for dispensing 1 μL volumes of aqueous LUV solution into a quartz cuvette filled with hexadecane. Images of the hanging droplets were collected once per second, and interfacial tension was calculated using Laplace-Young fitting in DataPhysics SCA20 software. Experiments were performed at room temperature.

3. Results and discussion

3.1. hDIB formation and electrical characterization

In addition to DPhPC-only DIBs that are well characterized [69–71], hDIBs with symmetric leaflet compositions were assembled in hexadecane oil with 300 nL droplets of LUV solution consisting of binary mixtures of DPhPC phospholipids and PBPEO diblock copolymers. The chemical structures for these amphiphiles are compared in Fig. S2 in the SI, and Table S2 in the SI shows that these solutions spontaneously reduce the interfacial tension from a value of ~45–50 mN/m for the neat oil-water interface within a few minutes, indicating the adsorption of amphiphiles and formation of well-packed monolayers [72]. At PBPEO fractions up to 15 mol%, which produced equilibrium monolayer tensions below 1 mN/m at the oil-water interface, we observed spontaneous bilayer formation between contacting droplets in hexadecane; i.e., no applied voltage was needed to induce bilayer thinning as previously observed with triblock BCPs [62]. However, unlike lipid-only DIBs that exhibit bilayer thinning within ~1 min, hDIBS often required >10 min for thinning to initiate after droplet contact. This delayed response is especially prominent at PBPEO molar ratios above 10 mol% in the LUVs. Interfacial thinning (and removal of excess oil) results in visual changes to the shared interface between droplets, as well as an increase in the amplitude of capacitive current induced by an AC voltage applied between the two supporting electrodes. In hexadecane, the area, A, (and thus the contact angle, θ) of the interface reached an equilibrium state within 60 s. Fig. 1A compares bottom-view images of a DPhPC-only DIB and an hDIB formed with 15 mol% PBPEO in the LUVs, both taken at their equilibrium zero-volt configurations. Compared to the DPhPC-only case, the addition of PBPEO resulted in a smaller equilibrium bilayer

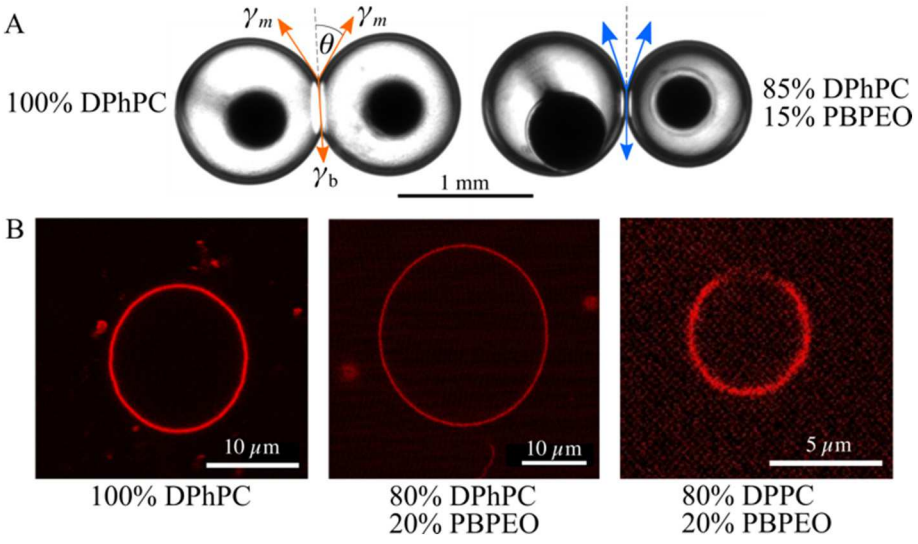

Fig. 1. Hybrid DIBs and GUVs. (A) bottom-view images of a DPhPC DIB (left) compared to an hDIB with 15 mol% PBPEO (right). (B) Confocal images near the equators of lipid-only and hybrid GUVs containing 0.1 mol% Nile Red. % denotes molar fractions.

area and lower contact angle (see Fig. 3A). Though the proportion of PBPEO in the droplet interface may differ from that found in the LUVs, we denote hDIB compositions from here on using the molar ratio of polymers to lipids in LUVs, as is common in describing DIBs from mixtures of species [73,74].

At PBPEO molar fractions >15 mol%, contacting droplets routinely coalesced (i.e., no stable membrane was formed) either before or shortly after thinning began. This same result was observed for 100 % PBPEO LUV solutions, which is consistent with the finding that polymer-only monolayers display higher values of equilibrium monolayer tension (>5 mN/m, Table S2) at the hexadecane water interface, indicating a lower packing density is obtained with only PBPEO amphiphiles. Lower monolayer tensions correspond to higher packing density, a requirement for stabilizing a bilayer between droplets [72]. Alternatively, we found that incorporating PBPEO into the oil phase instead resulted in an average equilibrium tension of only ~0.5 mN/m (Table S2). Yet, while putting DPhPC lipids in hexadecane is a viable route to forming a DIB, droplets submerged in PBPEO-hexadecane did not connect to form a thinned bilayer, even under the application of voltage. Therefore, ensuing measurements focus solely on hDIBs formed with aqueous LUV solutions at PBPEO molar ratios from 0 to 15 mol%.

To approximate how PL and BCP distribute in an hDIB, we assembled and imaged giant unilamellar vesicles (GUVs) from mixtures of the two species and added 0.1 mol% Nile Red, a lipophilic fluorescent dye. As control cases, DPhPC vesicles were found to be uniformly fluorescent (Fig. 1B), while PBPEO-only GUVs exhibited no fluorescence, despite being visible in brightfield with phase contrast (Fig. S3). For the latter, the dye precipitated into irregular clumps in the viewing chamber. However, mixtures of lipids and PBPEO were observed to be fluorescent, either uniformly or locally depending on the lipid type. Vesicles appeared uniformly fluorescent at the tested molar ratios of 5 %, 10 %, 20 %, 50 %, and 80 % PBPEO (Figs. 1B, and S4–S6) when PBPEO was combined with DPhPC, and we found no evidence of GUVs visible only in brightfield and not in fluorescence mode, which would have occurred if there were PBPEO-only vesicles present. This was true even at a PBPEO concentration of 80 mol% (Fig. S4), where PBPEO outnumber DPhPC 4:1. The observation that fluorescence intensity is noticeably lower for GUVs with 80 mol% versus 20 mol% PBPEO (Fig. S6) shows that more PBPEO leads to less Nile Red in the vesicle and a weaker fluorescent signal. In contrast, we observed locally non-fluorescent regions in GUVs comprised of 20 mol% PBPEO and 80 mol% DPPC (Fig. 1B), suggesting co-existing lipid-rich (fluorescent) and polymer-rich (non-fluorescent) regions in these membranes. Phase separation was routinely observed in many (n>10) separate DPPC:PBPEO GUVs (Fig. S7), which we qualitatively confirmed by viewing multiple vertical slices on separate GUVs. Phase separation in hybrid vesicles is common, especially when a high melting point lipid such as DPPC is used [26,35,38].

Therefore, in combination with our finding that mixtures of DPhPC and PBPEO (even at high BCP:PL ratios) do not produce visible non-fluorescent GUVs, we conclude that PBPEO is present in the GUVs and that DPhPC and PBPEO are evenly mixed. Thus, we expect DIBs formed from mixed vesicles to consist of similar BCP:PL ratios and remain homogeneously mixed. Mixing of these constituents makes sense given that DPhPC is in a liquid crystalline fluid phase at room temperature [75] and the low molecular weight of the PBPEO polymer chosen for this work is expected to minimize the difference in hydrophobic thickness that can drive phase separation. Homogeneous mixing of PC lipids and low molecular weight PBPEO was also observed in vesicles by Senevirratne et al. [76] and Lim et al. [27]. Similarly, Gettel et al. [28] and Bieligmeyer et al. [32] separately observed that low molecular weight PIPEO diblock copolymers form well-mixed hybrid bilayers when combined with low melting point POPC and DPhPC lipids, respectively.

To evaluate the equivalent electrical parameters and assess structural differences in DPhPC-based hDIBs, we applied a 10 mV, 10 Hz triangular voltage waveform between connected droplets and measured the induced square-wave current using a patch-clamp amplifier. As discussed elsewhere [70], the square wave current response can be analyzed to extract nominal values of bilayer resistance, R, and capacitance, C. A DC voltage can also be superimposed onto the AC signal to evaluate these quantities at nonzero average transmembrane potentials. Bottom view images of the connected droplets are intermittently obtained during electrical measurements to assess A and θ versus membrane composition and applied voltage.

Fig. 2A and Table 1 present average values of specific membrane resistance, R_m ($R_m = R \times A$), measured at 0 and 200 mV DC for varying percentages of PBPEO. Across all compositions, we observe values of specific resistance on the order of 1–25 MΩ cm^2, which indicates that both lipid-only and hybrid interfaces create effective ionic seals between droplets. At 0 mV DC, the data show that 5 mol% and 10 mol% PBPEO reduce the average value of R_m below that measured for DPhPC-only, whereas 15 mol% increases R_m above that for the control case. These values of R_m correspond to very large nominal values of R (~10 GΩ) and, thus, very small amplitudes of measured ohmic current (<1pA). Similarly, Bieligmeyer et al. recorded membrane resistances >10 GΩ in homogeneously mixed suspended membranes built from DPhPC and PIPEO [32]. However, increasing the transmembrane potential to 200 mV significantly reduces the values of specific resistance (possibly due to electroporation aided by voltage-induced thinning or electrowetting-driven reductions in membrane tension). PBPEO-induced reductions in R_m (at both 0 and 200 mV DC) are consistent with results from Paxton et al. [36], who demonstrated that mixtures of DOPC and PBPEO (MW = 2.9 kDa) are more permeability to ions compared to lipid-only or polymer-only membranes. Still, all values of R_m measured here remain above 1 MΩ cm^2, and there is no clear trend that increasing amounts of PBPEO lowers the specific resistance under applied voltage.

Similarly, Fig. 2B and Table 1 compare the average values of specific capacitance, C_m ($C_m = \delta C/\delta A$), measured for hDIBs with various percentages of PBPEO. Specific capacitance is determined as described elsewhere [70]. These data reveal that hDIBs containing up to 10 mol% PBPEO exhibit values of C_m similar to DPhPC-only DIBs at 0 mV DC (C_m = 0.65 μF/cm^2 [70]). Since C_m represents the ratio of dielectric permittivity, ϵ, to hydrophobic thickness, t, matching values of C_m and similar hydrophobic region dielectric constants (2.2 for DPhPC [70] vs. 2.5 for PB [77]) imply that hDIBs formed with 10 mol% or less PBPEO have similar hydrophobic thicknesses at 0 mV (Table 1). However, at 15 mol% PBPEO, the value of C_m measured at 0 mV DC decreases to ~0.56 μF/cm^2, which corresponds to a 3-4 Å increase in hydrophobic thickness. The fact that C_m reduces only slightly at higher mol% is consistent with work by Shen, et al. who measured the hydrophobic thickness of PB_{12}-*b*-PEO_8 bilayers to be 5.1 nm [78], which would have an equivalent C_m value of ~0.38 μF/cm^2. A number weighted average value of C_m for 15 mol% PBPEO and 85 mol% DPhPC is 0.61 μF/cm^2, close to the average C_m reported herein.

Additionally, measurements of C_m at 200 mV DC are used to gauge changes in thickness due to voltage-induced oil exclusion or bilayer compression [54,71]. All membrane types show higher values of C_m at 200 mV DC compared to their respective values at 0 mV DC, and the largest increase is observed for 15 mol% PBPEO, where C_m increases to an average value of ~0.62 μF/cm^2. This higher sensitivity to voltage correlates to the larger initial (zero-volt) thickness, and it suggests that a greater amount of oil exclusion or membrane compression can occur when approximately 1 in 7 molecules in the membrane is PBPEO. Unfortunately, we failed to form bilayers with a PBPEO composition higher than 15 mol%. Therefore, it remains unknown how much thicker a PBPEO-only bilayer would be or how much its thickness decreases when a DC voltage is applied.

3.2. Equilibrium energetics of hDIBs

As observed in the image of 15 mol% PBPEO hDIB in Fig. 1A, the presence of PBPEO in the interface results in adhered droplets with

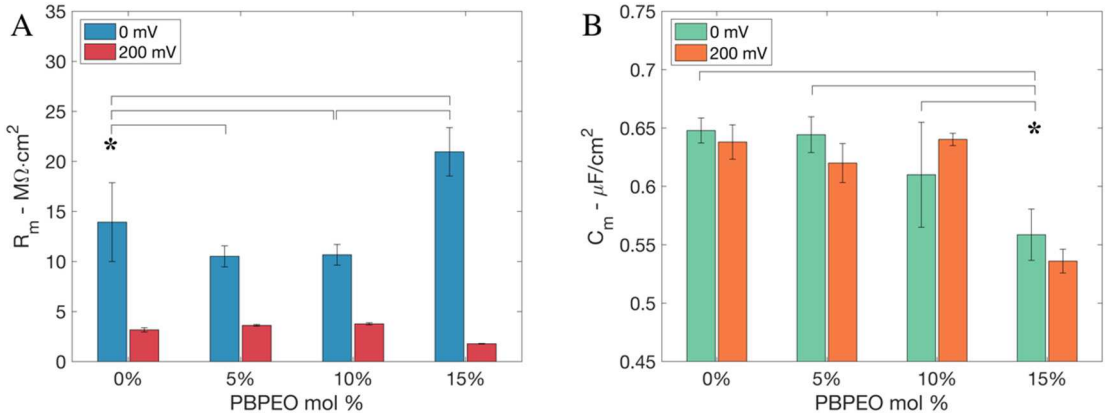

Fig. 2. Electrical properties of hDIBs. (A) Membrane resistance measured at 0 mV (blue, $n = 7$) and 200 mV (red, $n = 5$). (B) Specific capacitance at 0 mV (green) and 200 mV (orange). Error bars represent one standard deviation; * denotes significant differences, where $p < 0.05$.

Table 1
Summary of measured hDIB physical parameters[a] at 0 mV.

PBPEO mol%	Specific resistance, R_m [MΩ·cm^2]	Specific capacitance, C_m [μF/cm^2]	Hydrophobic thickness,[b] t [Å]	Contact angle, θ_0[°]	Monolayer tension, γ_m [N/m]	Bilayer tension, γ_b [N/m]	Free energy of formation, ΔF [mJ/m^2]
0	13.9 ± 3.92	0.65 ± 0.01	30.00 ± 0.04	33.5 ± 0.33	0.95 ± 0.10	1.58 ± 0.10	0.31 ± 0.03
5	10.5 ± 1.04	0.64 ± 0.02	30.46 ± 0.06	30.7 ± 0.27	0.90 ± 0.06	1.56 ± 0.05	0.25 ± 0.02
10	10.7 ± 1.03	0.62 ± 0.04	31.34 ± 0.21	26.8 ± 2.14	0.70 ± 0.09	1.31 ± 0.08	0.15 ± 0.04
15	21.0 ± 2.40	0.56 ± 0.47	34.81 ± 0.13	25.1 ± 1.60	0.53 ± 0.09	0.96 ± 0.08	0.09 ± 0.01

[a] Average values and standard deviations computed from $n \geq 5$ independent measurements.
[b] Computed from values of C_m using a value of 2.2 for the dielectric constant.

smaller values of contact area and contact angle at 0 mV than are observed for a DPhPC-only DIB. Fig. 3A confirms this trend, showing that the average contact angle at 0 mV, θ_0, decreases linearly from 34° at 0 mol% PBPEO to ~24° at 15 mol% PBPEO. This reduction in contact reflects a lower gain in free energy through spontaneous adhesion [79]. To quantify how much the PBPEO alters the tensions of the monolayers, γ_m, and bilayer, γ_b, and the resulting adhesive energy describing the connected droplet pair, we employed an established technique [70] to first determine equilibrium values of γ_m. This is achieved by measuring changes in θ caused by applied voltage.

Due to electrowetting, an applied voltage charges the capacitive interface and lowers γ_b [70]. This relaxation in bilayer tension leads to concomitant increases in contact area and angle needed to satisfy the three-force balance (Fig. 1A) and conserve the fixed droplet volumes. Fig. 3B shows these changes in contact angle due to electrowetting, quantified as the change in the cosine of θ versus the square of the applied DC voltage for each membrane type. These data exhibit linear relationships, where the slope for a given series is governed by the ratio $C_m/4\gamma_m$. Therefore, performing a linear regression on each data series resulted in values of slope for each membrane composition that were used with their corresponding value of C_m (Table 1) to determine average values of γ_m [30]. Fig. 3C and Table 1 show that γ_m decreases from 0.95 mN/m for a DPhPC-only DIB to ~0.56 mN/m for a DIB containing 15 mol% PBPEO. These differences in γ_m show that PBPEO molecules present in the membrane reduce interactions between oil and water molecules at the droplet surfaces. This could stem from hydrophobic PB blocks increasing the lateral packing density of amphiphiles in the monolayers or hydrophilic PEO blocks adopting mushroom like conformations that shield the hydrophobic lipid tails from water. Spectroscopy techniques such as vibrational sum frequency generation [80,81] could be used to reveal PBPEO's specific mechanisms of action.

The zero-volt tension of the bilayer γ_b was then computed using:

$$\gamma_b = 2\gamma_m cos\theta_0. \quad (1)$$

Values reported in Table 1 show that PBPEO in the interface lowers the γ_b by an amount proportional to the molar percentage of PBPEO. Thus, these measurements reveal that an hDIB formed by DPhPC and PBPEO has a similar hydrophobic thickness but a reduced lateral tension, a relationship that may affect the interactions of membrane-active species, such as transmembrane channels or engineered particles.

Finally, the free energy of formation, ΔF, was calculated using:

$$\Delta F = 2\gamma_m - \gamma_b \quad (2)$$

This quantity reflects the reduction in free energy of the system gained by replacing the opposing monolayer-coated regions of the droplets with a shared bilayer interface. Alternatively, it can be interpreted as the energy per unit area (mN/m = mJ/m^2) required to separate the attached droplets. The specific value of ΔF is strongly dependent on both the choice of surfactant and oil [62,79]. Here, the ΔF data in Fig. 3D and Table 1 show that increasing the mol% of PBPEO reduces the free energy of formation from ~0.3 mJ/m^2 for 0 mol% PBPEO to ~0.1 mJ/m^2 at 15 mol% PBPEO (a 66 % reduction). Despite lower values of γ_m corresponding to bilayers containing PBPEO (a factor itself that can reduce ΔF), this trend suggests that DPhPC:PBPEO monolayers favor interactions with hexadecane molecules over those with an opposing monolayer of DPhPC:PBPEO. This trend is revealed in the data as well; the free energy gained during bilayer formation is a larger percentage of the monolayer tension when PBPEO is absent ($\Delta F/\gamma_m$~33% for 0 mol% PBPEO) versus when it is present ($\Delta F/\gamma_m$~17% for 15 mol% PBPEO). More-favorable surfactant-oil interactions can also lead to a greater amount of oil retained in the membrane after thinning, a result that is consistent with the reduction in C_m (and the increase in t) observed for hDIBs containing 15 mol% PBPEO.

3.3. Ion channel formation and hDIB stability under applied voltage

The prior sections examined changes in membrane structure and DIB energetics when PBPEO is present in both leaflets of the bilayer. Because the addition of PBPEO to DPhPC DIBs results in an increase in average hydrophobic thicknesses of <15 mol%, homogeneous mixing of the two

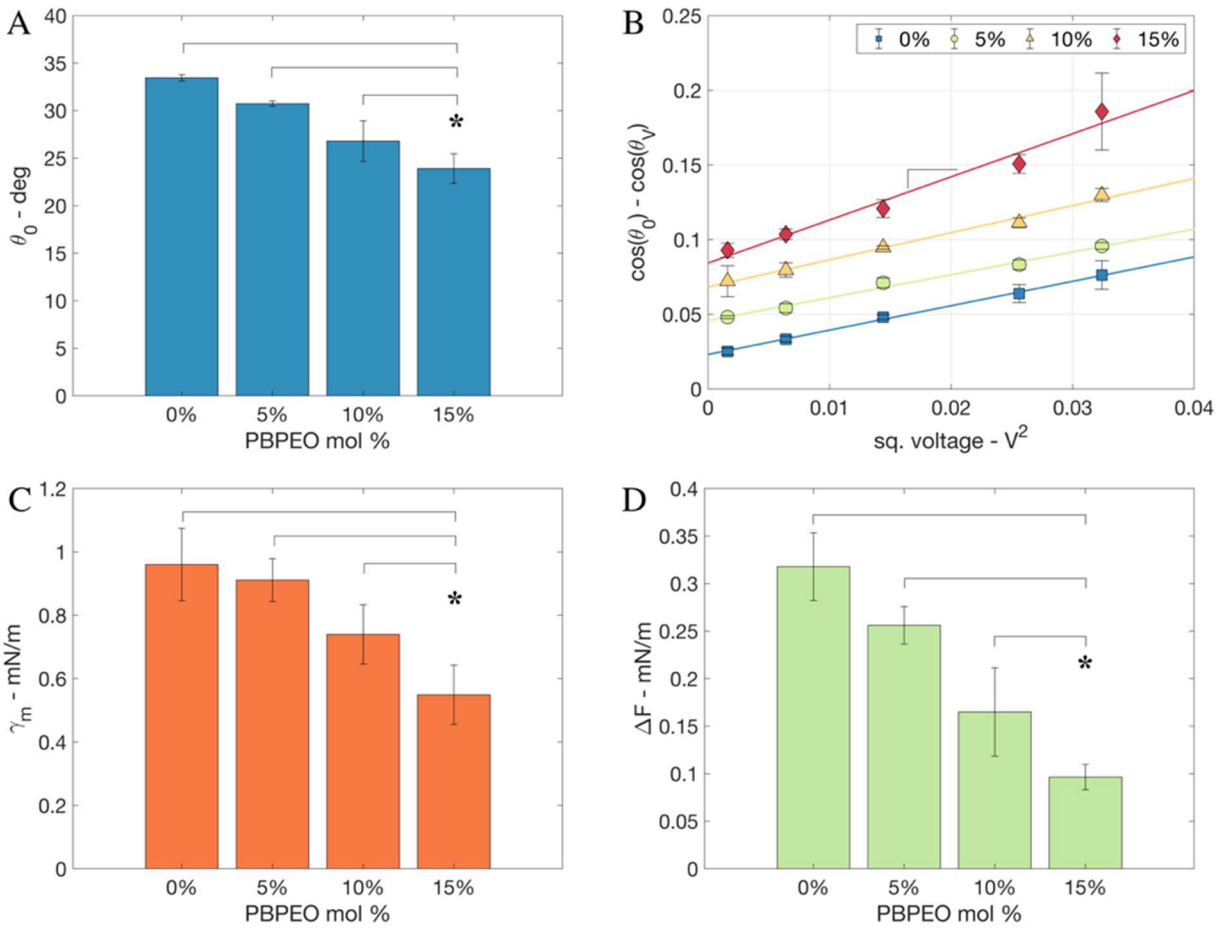

Fig. 3. Energetics of hDIBs. (A) Contact angles measured at 0 mV. (B) The change in the cosine of the contact angle versus the square of the applied voltage for different PBPEO mol% in DPhPC. Data have been offset vertically for clarity of presentation. (C) In situ monolayer tensions calculated from the slopes obtained in (B). (D) Free energy of formation at 0 mV determined from monolayer tensions in (C) and contact angles in (A). A minimum of $n = 5$ measurements were made of each quantity; error bars represent one standard deviation.

components, and reduced membrane tension, we hypothesized these conditions may affect the voltage-driven insertion and ion channel formation of alamethicin (alm) peptides. To test this hypothesis, we performed cyclic voltammetry (CV) measurements on hDIBs of varying mol % of PBPEO with 0.5 μM alm added to both droplets.

Representative measurements of bilayer area-normalized ion currents versus applied voltage (120 mV amplitude, 10 mHz sinusoidal waveform) are shown in Fig. 4A. The low current densities at voltages below 80 mV correspond to alm residing in a surface-bound state on the membrane [82,83]. At higher applied voltages, however, alm peptides are driven into the membrane, where they oligomerize and form conductive channels with neighboring monomers. This change of

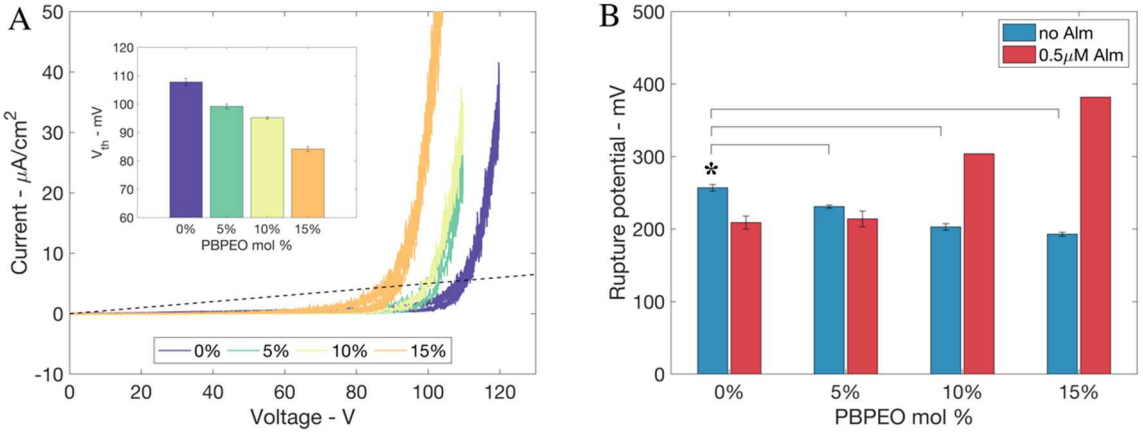

Fig. 4. Behavior of alm in hDIBs. (A) Current-voltage curves of hDIBs with 0.5 μM alamethicin added to both droplets. Each current response is normalized by the initial membrane area at zero volts. The black dashed line represents the specific conductance threshold (100 μS/cm^2) used to determine the voltage threshold for alamethicin insertion. Inset: Voltage threshold versus PBPEO mol% ($n = 5$). (B) Bar graphs of the average rupture potential ($n = 5$) measured with (0.5 μM) and without alamethicin versus PBPEO mol%. Error bars represent one standard deviation.

conformation by many alm peptides leads to an exponential increase in the measured ion current [52,84], as is observed in Fig. 3A at voltages near 100 mV. The voltage threshold, V_{th}, is a thermodynamic parameter dependent on peptide concentration, temperature, and membrane fluidity, tension, and thickness [73,83,85]. V_{th} can be quantified and compared across measurements by locating the voltage at which the conductance of the bilayer increases above an arbitrary level. Herein, we select 100 μS/cm^2 as the threshold specific conductance for the membrane (shown as a dashed line) [86].

Fig. 4 shows that an increased mol% of PBPEO leads to a lower intersection voltage between the measured current density and the threshold conductance. Specifically, V_{th} for 15 mol% PBPEO is 92 mV, versus 111 mV for 0 mol% PBPEO. This difference means that alm inserts and oligomerizes in a homogeneously-mixed hDIB more easily (i.e., at lower voltage) than in a DPhPC-only bilayer; i.e. there is a lower barrier to insertion and oligomerization. Alamethicin insertion into fluid, homogeneous hybrid bilayers is consistent with the finding that OmpF channels insert into the fluid polymer-rich domains of phase-separated hybrid bilayers as observed by Thoma et al. [38]. While it is known that negatively charged membranes enhance alm insertion [87], we do not consider this to be a factor here since Table S1 shows that the addition of PBPEO into the DPhPC vesicles did not significantly change the surface potential of hybrid vesicles supplied for bilayer formation. An alternative reason for the drop-in V_{th} is that macromolecular crowding (caused by the hydrated PEO groups) enhances peptide association on the membrane [88]—an increase in peptide concentration corresponds to an apparent reduction threshold voltage. Also, it may be that PEO groups extending past the lipid head groups blanket nearby regions of the membrane, which causes alm to adsorb in higher concentrations in remaining unshielded areas. This rationale was used previously to explain the delay in alamethicin channel formation at a fixed voltage observed in PMOXA-PDMS-PMOXA polymer membranes [13]. A third possibility is that PBPEO interspersed in the membrane changes the fluidity of the bilayer as observed by Seneviratne et al. [76]. Nonetheless, the trend shows that the PEO hydrophilic groups, which extend past the phosphate head groups of the lipids into the bulk aqueous phase, do not fully inhibit membrane association necessary for alm insertion into homogeneously mixed membranes. Thus, these measurements on alm show proof of concept that BCPs can be used to tune membrane properties in ways that could assist the interactions of other membrane-active species.

We observed a second change caused by PBPEO in alm-doped hDIBs. Fig. 4B presents bar graphs of the average rupture potential of DIBs with (0.5 μM) and without alamethicin versus the percentage of PBPEO. Membrane rupture occurs when an electric field creates and drives unstable growth in voltage-induced pores (or defects) through the membrane [89]. The rupture potential for each composition was recorded when the two droplets coalesced under a slowly increasing DC voltage. Without PBPEO, the average rupture potential of a DPhPC DIB with and without alm is statistically similar (~250 mV). However, as PBPEO% increases, the average rupture potential decreases steadily in the absence of alm (~200 mV for 15 mol% PBPEO). The energy required to increase the size of a voltage-induced pore in the bilayer, and thus drive it to an unstable state that causes rupture, is proportional to membrane tension [89]. Therefore, the reduced rupture potentials of hDIBS correlate to the PBPEO-induced reductions in bilayer tension reported in Table 1. This relationship shows that the presence of PBPEO in the membrane, and its corresponding disordering effect on DPhPC tails, fails to equally penalize electroporation, which results in a lower rupture voltage. However, this relationship also suggests that the maximum rupture potential of a hDIB could be increased by understanding and controlling the lateral organization of lipids and diblocks in a bilayer. For example, some combinations of hybrid membrane constituents enhance molecular packing, as seen when cholesterol is added to bilayers constructed from low-melting-point lipids [90].

In contrast, the rupture potential *increases* steadily when alm peptides are present. No error bars are provided for the 10 mol% and 15 mol% conditions because membranes were still intact despite the measured current exceeding the limits of measurement equipment; the reported rupture potential values for these conditions are therefore lower limits. However, the fact that rupture occurred at potentials well above 300 mV for these higher fractions of PBPEO strongly demonstrates the opposite trend. While the cause of this result is not fully understood, it appears to indicate a collective stabilizing effect caused by PBPEO and alm in the membrane. Differences in bilayer tensions, including under high voltages, may be a reason. Unfortunately, our method for extracting monolayer tension via changes in contact angle versus voltage is not well suited to assessing the tensions in alm-doped membranes due to the difficulty in measuring C_m at voltages where ion channels are open and the conductance of the membrane is high. Moreover, due to the fact that membranes containing PBPEO exhibit lower threshold voltages for alm insertion, which leads to larger currents at a particular voltage, the resistance to rupture may be helped by more open ion channels in the bilayer. Nonetheless, this result adds to the possibility that doping lipid membranes with amphiphilic diblock copolymers can be used to augment the properties of a membrane while retaining a sufficiently biomimetic structure and function.

4. Conclusions

Herein, we examined the effects of adding a low molecular weight diblock copolymer amphiphile into lipid bilayers assembled between aqueous droplets in oil. We found that DPhPC DIBs doped with 0–15 mol % PBPEO form homogeneously mixed hybrid bilayers. These hybrid membranes demonstrated similar (within 0 to +20 %) average hydrophobic thickness to lipid-only DIBs, are leak-free to ion transport and are stable under applied potentials, which enabled a comprehensive assessment of the effects of added PBPEO on the physical properties of the interfacial bilayer. Our data show that increasing the fraction of PBPEO lowers both the monolayer and bilayer tensions by nearly 50 % compared to DPhPC DIBs in hexadecane. Also, the energy of adhesion fell by 66 % for 15 mol% PBPEO, which explains the reduced contact areas between droplets. It was also observed that an increased percentage of PBPEO in hDIBs reduces the voltage threshold for alamethicin channel formation and raises the rupture potential of membranes containing alm.

These results show proof of concept that BCPs can be used to selectively preserve and modulate the properties of hybrid membranes in ways that favor the interactions of other membrane-active species, yet also make them stable at higher voltages. These improvements, when combined with targeted studies of membrane permeability, could lead to further tunability of biomimetic membranes, such as enabling the development of bioelectronic devices for sensing, signal processing, and selective transport via ion-channels. Finally, this work also motivates research to better understand conditions and polymer architectures that allow for polymer-only DIBs with similar thickness to lipid membranes but significantly greater mechanical durability and resistance to chemical degradation.

CRediT authorship contribution statement

S. Koner: Conceptualization, Investigation, Formal analysis, Writing – Original draft. **J. Tawfik:** Investigation. **F. Mashali:** Conceptualization, Investigation. **K. Kennison:** Investigation. **W. McClintic:** Investigation. **F. Heberle:** Formal analysis, Writing – Review & editing. **Y-M. Tu:** Investigation. **M. Kumar:** Resources. **S. Sarles:** Conceptualization, Formal Analysis, Visualization, Writing – Review & editing.

Declaration of competing interest

The authors declare that they have no known competing financial interests or personal relationships that could have appeared to influence

the work reported in this paper.

Data availability

Data will be made available on request.

Acknowledgments

This work was supported by the National Science Foundation [CBET-1752197, CMMI-2119718] and the Air Force Office of Scientific Research [FA9550-19-1-0213]. S. Koner acknowledges financial support from the Center for Materials Processing at the University of Tennessee, Knoxville. In the Kumar Lab, work on this project was supported by National Science Foundation through the Center for Dynamics and Control of Materials (CDCM) Materials Research Science and Engineering Center (MRSEC) (DMR-1720595) and through an NSF DMREF grant (CMMI-2119716).

Appendix A. Supplementary data

Supplementary data to this article can be found online at https://doi.org/10.1016/j.bbamem.2022.183997.

References

[1] Y. Zhang, S. Inal, C.-Y. Hsia, M. Ferro, M. Ferro, S. Daniel, R.M. Owens, Supported lipid bilayer assembly on PEDOT:PSS films and transistors, Adv. Funct. Mater. 26 (2016) 7304–7313.
[2] C.M. Jewell, J.-M. Jung, P.U. Atukorale, R.P. Carney, F. Stellacci, D.J. Irvine, Oligonucleotide delivery by cell-penetrating "Striped" nanoparticles, Angew. Chem. Int. Ed. 50 (2011) 12312–12315.
[3] A. Verma, O. Uzun, Y. Hu, Y. Hu, H.-S. Han, N. Watson, S. Chen, D.J. Irvine, F. Stellacci, Surface-structure-regulated cell-membrane penetration by monolayer-protected nanoparticles, Nat. Mater. 7 (2008) 588–595.
[4] Y. Astier, O. Braha, H. Bayley, Toward single molecule DNA sequencing: direct identification of ribonucleoside and deoxyribonucleoside 5'-monophosphates by using an engineered protein nanopore equipped with a molecular adapter, J. Am. Chem. Soc. 128 (2006) 1705–1710.
[5] H. Bayley, I. Cazimoglu, C.E.G. Hoskin, Synthetic tissues, Emerg. Top. Life Sci. 3 (2019) 615–622.
[6] W. Song, H. Joshi, R. Chowdhury, J.S. Najem, Y.-X. Shen, C. Lang, C.B. Henderson, Y.-M. Tu, M. Farell, M.E. Pitz, C.D. Maranas, P.S. Cremer, R.J. Hickey, S.A. Sarles, J.-L. Hou, A. Aksimentiev, M. Kumar, Artificial water channels enable fast and selective water permeation through water-wire networks, Nat. Nanotechnol. 15 (2020) 73–79.
[7] M. Kumar, M. Grzelakowski, J. Zilles, M. Clark, W. Meier, Highly permeable polymeric membranes based on the incorporation of the functional water channel protein aquaporin Z, Proc. Natl. Acad. Sci. 104 (2007) 20719–20724.
[8] C.Y. Tang, Y. Zhao, R. Wang, C. Hélix-Nielsen, A.G. Fane, Desalination by biomimetic aquaporin membranes: review of status and prospects, Desalination 308 (2013) 34–40.
[9] A.L. Ottova, H. Ti Tien, Self-assembled bilayer lipid membranes: from mimicking biomembranes to practical applications, Bioelectrochem. Bioenerg. 42 (1997) 141–152.
[10] P.S. Cremer, S.G. Boxer, Formation and spreading of lipid bilayers on planar glass supports, J. Phys. Chem. B 103 (1999) 2554–2559.
[11] C. Nardin, M. Winterhalter, W. Meier, Giant free-standing ABA triblock copolymer membranes, Langmuir 16 (2000) 7708–7712.
[12] D.E. Discher, A. Eisenberg, Polymer vesicles, Science 297 (2002) 967–973.
[13] D. Wong, T.-J. Jeon, J. Schmidt, Single molecule measurements of channel proteins incorporated into biomimetic polymer membranes, Nanotechnology 17 (2006) 3710.
[14] S. Belegrinou, J. Dorn, M. Kreiter, K. Kita-Tokarczyk, E.-K. Sinner, W. Meier, Biomimetic supported membranes from amphiphilic block copolymers, Soft Matter 6 (2010) 179–186.
[15] A. Krywko-Cendrowska, S. di Leone, M. Bina, S. Yorulmaz-Avşar, C.G. Palivan, W. Meier, Recent advances in hybrid biomimetic polymer-based films: from assembly to applications, Polymers 12 (2020).
[16] Y.K. Go, C. Leal, Polymer-lipid hybrid materials, Chem. Rev. 121 (2021) 13996–14030.
[17] T. Ruysschaert, A.F.P. Sonnen, T. Haefele, W. Meier, M. Winterhalter, D. Fournier, Hybrid nanocapsules: interactions of ABA block copolymers with liposomes, J. Am. Chem. Soc. 127 (2005) 6242–6247.
[18] J. Kowal, X. Zhang, I.A. Dinu, C.G. Palivan, W. Meier, Planar biomimetic membranes based on amphiphilic block copolymers, ACS Macro Lett. 3 (2014) 59–63.
[19] A. Gonzalez-Perez, V. Castelletto, I.W. Hamley, P. Taboada, Biomimetic triblock copolymer membranes: from aqueous solutions to solid supports, Soft Matter 7 (2011) 1129–1138.
[20] H.L. Wang, T.-S. Chung, Y.W. Tong, K. Jeyaseelan, A. Armugam, H.H.P. Duong, F. Fu, H. Seah, J. Yang, M. Hong, Mechanically robust and highly permeable AquaporinZ biomimetic membranes, J. Membr. Sci. 434 (2013) 130–136.
[21] S. Winzen, M. Bernhardt, D. Schaeffel, A. Koch, M. Kappl, K. Koynov, K. Landfester, A. Kroeger, Submicron hybrid vesicles consisting of polymer–lipid and polymer–cholesterol blends, Soft Matter 9 (2013) 5883–5890.
[22] M. Garni, S. Thamboo, C.-A. Schoenenberger, C.G. Palivan, Biopores/membrane proteins in synthetic polymer membranes, Biochim. Biophys. Acta Biomembr. 2017 (1859) 619–638.
[23] Z. Cheng, A. Tsourkas, Paramagnetic porous polymersomes, Langmuir 24 (2008) 8169–8173.
[24] K. Kita-Tokarczyk, F. Itel, M. Grzelakowski, S. Egli, P. Rossbach, W. Meier, Monolayer interactions between lipids and amphiphilic block copolymers, Langmuir 25 (2009) 9847–9856.
[25] J. Nam, P.A. Beales, T.K. Vanderlick, Giant Phospholipid/Block copolymer hybrid vesicles: mixing behavior and domain formation, Langmuir 27 (2011) 1–6.
[26] M. Schulz, D. Glatte, A. Meister, P. Scholtysek, A. Kerth, A. Blume, K. Bacia, W. H. Binder, Hybrid lipid/polymer giant unilamellar vesicles: effects of incorporated biocompatible PIB–PEO block copolymers on vesicle properties, Soft Matter 7 (2011) 8100–8110.
[27] S.K. Lim, H.-P. De Hoog, A.N. Parikh, M. Nallani, B. Liedberg, Hybrid, nanoscale phospholipid/block copolymer vesicles, Polymers 5 (2013) 1102–1114.
[28] D.L. Gettel, J. Sanborn, M.A. Patel, H.-P. de Hoog, B. Liedberg, M. Nallani, A. N. Parikh, Mixing, diffusion, and percolation in binary supported membranes containing mixtures of lipids and amphiphilic block copolymers, J. Am. Chem. Soc. 136 (2014) 10186–10189.
[29] A. Balestri, L. Chiappisi, C. Montis, S. Micciulla, B. Lonetti, D. Berti, Organized hybrid molecular films from natural phospholipids and synthetic block copolymers: a physicochemical investigation, Langmuir 36 (2020) 10941–10951.
[30] J.Y. Kang, I. Choi, M. Seo, J.Y. Lee, S. Hong, G. Gong, S.S. Shin, Y. Lee, J.W. Kim, Enhancing membrane modulus of giant unilamellar lipid vesicles by lateral co-assembly of amphiphilic triblock copolymers, J. Colloid Interface Sci. 561 (2020) 318–326.
[31] N. Hamada, S. Gakhar, M.L. Longo, Hybrid lipid/block copolymer vesicles display broad phase coexistence region, Biochim. Biophys. Acta Biomembr. 1863 (2021), 183552.
[32] M. Bieligmeyer, F. Artukovic, S. Nussberger, T. Hirth, T. Schiestel, M. Müller, Reconstitution of the membrane protein OmpF into biomimetic block copolymer–phospholipid hybrid membranes, Beilstein J. Nanotechnol. 7 (2016) 881–892.
[33] C.W. Meuse, S. Krueger, C.F. Majkrzak, J.A. Dura, J. Fu, J.T. Connor, A.L. Plant, Hybrid bilayer membranes in air and water: infrared spectroscopy and neutron reflectivity studies, Biophys. J. 74 (1998) 1388–1398.
[34] T.P.T. Dao, F. Fernandes, M. Er-Rafik, R. Salva, M. Schmutz, A. Brûlet, M. Prieto, O. Sandre, J.F. Le Meins, Phase separation and nanodomain formation in hybrid Polymer/Lipid vesicles, ACS Macro Lett. 4 (2015) 182–186.
[35] J. Kowal, D. Wu, V. Mikhalevich, C.G. Palivan, W. Meier, Hybrid polymer-lipid films as platforms for directed membrane protein insertion, Langmuir 31 (2015) 4868–4877.
[36] W.F. Paxton, P.T. McAninch, K.E. Achyuthan, S.H.R. Shin, H.L. Monteith, Monitoring and modulating ion traffic in hybrid lipid/polymer vesicles, Colloids Surf. B: Biointerfaces 159 (2017) 268–276.
[37] S. Khan, M. Li, S.P. Muench, L.J.C. Jeuken, P.A. Beales, Durable proteo-hybrid vesicles for the extended functional lifetime of membrane proteins in bionanotechnology, Chem. Commun. 52 (2016) 11020–11023.
[38] J. Thoma, S. Belegrinou, P. Rossbach, M. Grzelakowski, K. Kita-Tokarczyk, W. Meier, Membrane protein distribution in composite polymer–lipid thin films, Chem. Commun. 48 (2012) 8811–8813.
[39] Z.A. Manzer, S. Ghosh, M.L. Jacobs, S. Krishnan, W.R. Zipfel, M. Piñeros, N. P. Kamat, S. Daniel, Cell-free synthesis of a transmembrane Mechanosensitive Channel protein into a hybrid-supported lipid bilayer, ACS Appl. Bio Mater. 4 (2021) 3101–3112.
[40] L. Ruiz-Pérez, C. Hurley, S. Tomas, G. Battaglia, Separating extreme pH gradients using amphiphilic copolymer membranes, ChemPhysChem 19 (2018) 1987–1989.
[41] H. Bayley, B. Cronin, A. Heron, M.A. Holden, W.L. Hwang, R. Syeda, J. Thompson, M. Wallace, Droplet interface bilayers, Mol. BioSyst. 4 (2008) 1191–1208.
[42] W.L. Hwang, M. Chen, B. Cronin, M.A. Holden, H. Bayley, Asymmetric droplet Interface bilayers, J. Am. Chem. Soc. 130 (2008) 5878–5879.
[43] M.A. Holden, D. Needham, H. Bayley, Functional bionetworks from nanoliter water droplets, J. Am. Chem. Soc. 129 (2007) 8650–8655.
[44] P. Mruetusatorn, G. Polizos, P.G. Datskos, G. Taylor, S.A. Sarles, J.B. Boreyko, D. G. Hayes, C.P. Collier, Control of membrane permeability in air-stable droplet Interface bilayers, Langmuir 31 (2015) 4224–4231.
[45] P.J. Milianta, M. Muzzio, J. Denver, G. Cawley, S. Lee, Water permeability across symmetric and asymmetric droplet Interface bilayers: interaction of cholesterol sulfate with DPhPC, Langmuir 31 (2015) 12187–12196.
[46] Z. Michalak, M. Muzzio, P.J. Milianta, R. Giacomini, S. Lee, Effect of monoglyceride structure and cholesterol content on water permeability of the droplet bilayer, Langmuir 29 (2013) 15919–15925.
[47] Z. Michalak, D. Fartash, N. Haque, S. Lee, Tunable crystallization via osmosis-driven transport across a droplet interface bilayer, CrystEngComm 14 (2012) 7865–7868.

[48] S.A. Sarles, J.D.W. Madden, D.J. Leo, Hair cell inspired mechanotransduction with a gel-supported, artificial lipid membrane, Soft Matter 7 (2011) 4644–4653.
[49] N. Tamaddoni, S.A. Sarles, Toward cell-inspired materials that feel: measurements and modeling of mechanotransduction in droplet-based, multi-membrane arrays, Bioinspiration Biomimetics 11 (2016), 036008.
[50] J. Xu, D.A. Lavan, Designing artificial cells to harness the biological ion concentration gradient, Nat Nano 3 (2008) 666–670.
[51] V. Restrepo Schild, M.J. Booth, S.J. Box, S.N. Olof, K.R. Mahendran, H. Bayley, Light-patterned current generation in a droplet bilayer array, Sci. Rep. 7 (2017) 46585.
[52] J.S. Najem, G.J. Taylor, R.J. Weiss, M.S. Hasan, G. Rose, C.D. Schuman, A. Belianinov, C.P. Collier, S.A. Sarles, Memristive Ion Channel-doped biomembranes as synaptic mimics, ACS Nano 12 (2018) 4702–4711.
[53] S. Koner, J.S. Najem, M.S. Hasan, S.A. Sarles, Memristive plasticity in artificial electrical synapses via geometrically reconfigurable, gramicidin-doped biomembranes, Nanoscale 11 (2019) 18640–18652.
[54] J.S. Najem, M.S. Hasan, R.S. Williams, R.J. Weiss, G.S. Rose, G.J. Taylor, S. A. Sarles, C.P. Collier, Dynamical nonlinear memory capacitance in biomimetic membranes, Nat. Commun. 10 (2019) 3239.
[55] J.J. Maraj, J.S. Najem, J.D. Ringley, R.J. Weiss, G.S. Rose, S.A. Sarles, Short-term facilitation-then-depression enables adaptive processing of sensory inputs by ion channels in biomolecular synapses, ACS Appl. Electron. Mater. 3 (10) (2021) 4448–4458, https://doi.org/10.1021/acsaelm.1c00610.
[56] G.J. Taylor, M.-A. Nguyen, S. Koner, E.C. Freeman, C.P. Collier, S.A. Sarles, Electrophysiological interrogation of asymmetric droplet interface bilayers reveals surface-bound alamethicin induces lipid flip-flop, Biochimica et Biophysica Acta (BBA) - Biomembranes 1861 (1) (2019) 335–343, https://doi.org/10.1016/j.bbamem.2018.07.001.
[57] M.-A. Nguyen, B. Srijanto, C.P. Collier, S.T. Retterer, S.A. Sarles, Hydrodynamic trapping for rapid assembly and in situ electrical characterization of droplet interface bilayer arrays, Lab Chip 16 (2016) 3576–3588.
[58] T.M. Schimel, M.-A. Nguyen, S.A. Sarles, S.C. Lenaghan, Pressure-driven generation of complex microfluidic droplet networks, Microfluid. Nanofluid. 25 (2021) 78.
[59] G. Villar, A.D. Graham, H. Bayley, A tissue-like printed material, Science 340 (2013) 48–52.
[60] E.J. Challita, J.S. Najem, R. Monroe, D.J. Leo, E.C. Freeman, Encapsulating networks of droplet Interface bilayers in a thermoreversible organogel, Sci. Rep. 8 (2018) 6494.
[61] M.J. Booth, I. Cazimoglu, H. Bayley, Controlled deprotection and release of a small molecule from a compartmented synthetic tissue module, Commun. Chem. 2 (2019) 142.
[62] N. Tamaddoni, G. Taylor, T. Hepburn, S. Michael Kilbey, S.A. Sarles, Reversible, voltage-activated formation of biomimetic membranes between triblock copolymer-coated aqueous droplets in good solvents, Soft Matter 12 (2016) 5096–5109.
[63] C. Basham, M. Pitz, J. Najem, S. Sarles, M.S. Hasan, Memcapacitive devices in neuromorphic circuits via polymeric biomimetic membranes, in: ASME 2019 Conference on Smart Materials, Adaptive Structures and Intelligent Systems, vol. ASME 2019 Conference on Smart Materials, Adaptive Structures and Intelligent Systems, 2019.
[64] S.S. Klara, P.O. Saboe, I.T. Sines, M. Babaei, P.-L. Chiu, R. DeZorzi, K. Dayal, T. Walz, M. Kumar, M.S. Mauter, Magnetically directed two-dimensional crystallization of OmpF membrane proteins in block copolymers, J. Am. Chem. Soc. 138 (2016) 28–31.
[65] Y.-M. Tu, W. Song, T. Ren, Y.-X. Shen, R. Chowdhury, P. Rajapaksha, T.E. Culp, L. Samineni, C. Lang, A. Thokkadam, D. Carson, Y. Dai, A. Mukthar, M. Zhang, A. Parshin, J.N. Sloand, S.H. Medina, M. Grzelakowski, D. Bhattacharya, W. A. Phillip, E.D. Gomez, R.J. Hickey, Y. Wei, M. Kumar, Rapid fabrication of precise high-throughput filters from membrane protein nanosheets, Nat. Mater. 19 (2020) 347–354.
[66] Y.-X. Shen, W. Song, D.R. Barden, T. Ren, C. Lang, H. Feroz, C.B. Henderson, P. O. Saboe, D. Tsai, H. Yan, P.J. Butler, G.C. Bazan, W.A. Phillip, R.J. Hickey, P. S. Cremer, H. Vashisth, M. Kumar, Achieving high permeability and enhanced selectivity for angstrom-scale separations using artificial water channel membranes, Nat. Commun. 9 (2018) 2294.
[67] G.J. Taylor, S.A. Sarles, Heating-enabled formation of droplet interface bilayers using Escherichia coli total lipid extract, Langmuir 31 (2014) 325–337.
[68] J. El-Beyrouthy, M.M. Makhoul-Mansour, G. Taylor, S.A. Sarles, E.C. Freeman, A new approach for investigating the response of lipid membranes to electrocompression by coupling droplet mechanics and membrane biophysics, J. R. Soc. Interface 16 (2019) 20190652.
[69] G.A. Venkatesan, S.A. Sarles, Droplet immobilization within a polymeric organogel improves lipid bilayer durability and portability, Lab Chip 16 (2016) 2116–2125.
[70] G.J. Taylor, G.A. Venkatesan, C.P. Collier, S.A. Sarles, Direct in situ measurement of specific capacitance, monolayer tension, and bilayer tension in a droplet interface bilayer, Soft Matter 11 (2015) 7592–7605.
[71] L.C.M. Gross, A.J. Heron, S.C. Baca, M.I. Wallace, Determining membrane capacitance by dynamic control of droplet Interface bilayer area, Langmuir 27 (2011) 14335–14342.
[72] G.A. Venkatesan, J. Lee, A.B. Farimani, M. Heiranian, C.P. Collier, N.R. Aluru, S. A. Sarles, Adsorption kinetics dictate monolayer self-assembly for both lipid-in and lipid-out approaches to droplet Interface bilayer formation, Langmuir 31 (2015) 12883–12893.
[73] G.J. Taylor, S.A. Sarles, Heating-enabled formation of droplet Interface bilayers using Escherichia coli Total lipid extract, Langmuir 31 (2015) 325–337.
[74] J.L. Korner, K.S. Elvira, The role of temperature in the formation of human–mimetic artificial cell membranes using droplet interface bilayers (DIBs), Soft Matter 17 (2021) 8891–8901.
[75] S. Kara, S. Afonin, O. Babii, A.N. Tkachenko, I.V. Komarov, A.S. Ulrich, Diphytanoyl lipids as model systems for studying membrane-active peptides, Biochim. Biophys. Acta Biomembr. 2017 (1859) 1828–1837.
[76] R. Seneviratne, R. Catania, M. Rappolt, L.J.C. Jeuken, P.A. Beales, Membrane mixing and dynamics in hybrid POPC/poly(1,2-butadiene-block-ethylene oxide) (PBd-b-PEO) lipid/block co-polymer giant vesicles, Soft Matter 18 (2022) 1294–1301.
[77] M. Pegoraro, K. Mitoraj, Dielectric properties of trans-1,4 polybutadiene, Makromol. Chem. 61 (1963) 132–138.
[78] Y.-X. Shen, W. Si, M. Erbakan, K. Decker, R. De Zorzi, P.O. Saboe, Y.J. Kang, S. Majd, P.J. Butler, T. Walz, Highly permeable artificial water channels that can self-assemble into two-dimensional arrays, Proc. Natl. Acad. Sci. 112 (2015) 9810–9815.
[79] P. Poulin, J. Bibette, Adhesion of water droplets in organic solvent, Langmuir 14 (1998) 6341–6343.
[80] C.M. Basham, U.I. Premadasa, Y.-Z. Ma, F. Stellacci, B. Doughty, S.A. Sarles, Nanoparticle-induced disorder at complex liquid-liquid interfaces: effects of curvature and compositional synergy on functional surfaces, ACS Nano 15 (2021) 14285–14294.
[81] A.U. Chowdhury, G.J. Taylor, V. Bocharova, R.L. Sacci, Y. Luo, W.T. McClintic, Y.-Z. Ma, S.A. Sarles, K. Hong, C.P. Collier, B. Doughty, Insight into the mechanisms driving the self-assembly of functional interfaces: moving from lipids to charged amphiphilic oligomers, J. Am. Chem. Soc. 142 (2020) 290–299.
[82] J.E. Hall, I. Vodyanoy, T.M. Balasubramanian, G.R. Marshall, Alamethicin. A rich model for channel behavior, Biophys. J. 45 (1984) 233–247.
[83] I. Vodyanoy, J.E. Hall, T.M. Balasubramanian, Alamethicin-induced current-voltage curve asymmetry in lipid bilayers, Biophys. J. 42 (1983) 71–82.
[84] T. Okazaki, M. Sakoh, Y. Nagaoka, K. Asami, Ion channels of alamethicin dimer N-terminally linked by disulfide bond, Biophys. J. 85 (2003) 267–273.
[85] S. Stankowski, U.D. Schwarz, G. Schwarz, Voltage-dependent pore activity of the peptide alamethicin correlated with incorporation in the membrane: salt and cholesterol effects, Biochim. Biophys. Acta Biomembr. 941 (1988) 11–18.
[86] G. Taylor, M.-A. Nguyen, S. Koner, E. Freeman, C.P. Collier, S.A. Sarles, Electrophysiological interrogation of asymmetric droplet interface bilayers reveals surface-bound alamethicin induces lipid flip-flop, Biochim. Biophys. Acta Biomembr. 2019 (1861) 335–343.
[87] F. Abbasi, J. Alvarez-Malmagro, Z. Su, J.J. Leitch, J. Lipkowski, Pore forming properties of alamethicin in negatively charged floating bilayer lipid membranes supported on gold electrodes, Langmuir 34 (2018) 13754–13765.
[88] W.T. McClintic, G.J. Taylor, M.L. Simpson, C.P. Collier, Macromolecular crowding affects voltage-dependent alamethicin pore formation in lipid bilayer membranes, J. Phys. Chem. B 124 (2020) 5095–5102.
[89] S.A. Freeman, M.A. Wang, J.C. Weaver, Theory of electroporation of planar bilayer membranes: predictions of the aqueous area, change in capacitance, and pore-pore separation, Biophys. J. 67 (1994) 42–56.
[90] M.A.S. Karal, M.K. Ahamed, N.A. Mokta, M. Ahmed, S. Ahammed, Influence of cholesterol on electroporation in lipid membranes of giant vesicles, Eur. Biophys. J. 49 (2020) 361–370.